Cell Research (2013) 23:274-289.

www.nature.com/cr

ORIGINAL ARTICLE

miR-486 sustains NF-κB activity by disrupting multiple NF-κB-negative feedback loops

Libing Song[1, *], Chuyong Lin[2, 3, *], Hui Gong[2, 3], Chanjuan Wang[2, 3], Liping Liu[1], Jueheng Wu[3, 4], Sha Tao[2, 3], Bo Hu[5], Shi-Yuan Cheng[5], Mengfeng Li[3, 4], Jun Li[2, 3]

[1]State Key Laboratory of Oncology in Southern China, Department of Experimental Research, Cancer Center, Sun Yat-sen University, Guangzhou, Guangdong 510060, China; [2]Department of Biochemistry, Zhongshan School of Medicine, Sun Yat-sen University, Guangzhou, Guangdong 510080, China; [3]Key Laboratory of Tropical Disease Control, Ministry of Education, Sun Yat-sen University, Guangzhou, Guangdong 510080, China; [4]Department of Microbiology, Zhongshan School of Medicine, Sun Yat-sen University, Guangzhou, Guangdong 510080, China; [5]Department of Neurology, Brain Tumor Institute, Robert H. Lurie Comprehensive Cancer Center, Northwestern University Feinberg School of Medicine, Chicago, IL 60827, USA

Deubiquitinases, such as CYLD, A20 and Cezanne, have emerged as important negative regulators that balance the strength and the duration of NF-κB signaling through feedback mechanisms. However, how these serial feedback loops are simultaneously disrupted in cancers, which commonly exhibit constitutively activated NF-κB, remains puzzling. Herein, we report that miR-486 directly suppresses NF-κB-negative regulators, CYLD and Cezanne, as well as multiple A20 activity regulators, including ITCH, TNIP-1, TNIP-2 and TNIP-3, resulting in promotion of ubiquitin conjugations in NF-κB signaling and sustained NF-κB activity. Furthermore, we demonstrate that upregulation of miR-486 promotes glioma aggressiveness both *in vitro* and *in vivo* through activation of NF-κB signaling pathway. Importantly, miR-486 levels in primary gliomas significantly correlate with NF-κB activation status. These findings uncover a novel mechanism for constitutive NF-κB activation in gliomas and support a functionally and clinically relevant epigenetic mechanism in cancer progression.

***Keywords*:** miR-486; NF-κB; ubiquitin; aggressiveness; gliomas

Cell Research (2013) **23**:274-289. doi:10.1038/cr.2012.174; published online 18 December 2012

Introduction

Since the discovery that the ubiquitin proteasome system is involved in the degradation of the natural inhibitors of nuclear factor-κB (NF-κB), IκBs, ubiquitin modification was shown to play roles in activation of NF-κB [1-3]. Besides simply prompting IκBs destruction, ubiquitination has been demonstrated to be a critical regulatory mechanism controlling the NF-κB signaling pathway. A growing number of proteins in the NF-κB signal transduction pathway have been identified to be modified by or to interact with ubiquitin. Notably, deregulation of ubiquitin conjugation/deconjugation in NF-κB signaling is frequently found in various human cancer types [4-7].

Ubiquitin conjugation, occurring at multiple steps within the NF-κB signaling cascades, serves as a positive regulator in NF-κB activation [4, 5]. For instance, TNF-α binding to TNFR leads to rapid recruitment of the adaptor protein TRADD, TNFR-associated factors TRAF2 and TRAF5, cellular inhibitor of apoptosis proteins c-IAP1 and c-IAP2, and receptor-interacting protein kinase (RIP1), resulting in autoubiquitination of TRAF2 and/or cIAP1 and K63-linked polyubiquitination of RIP1 [8-10]. K63-linked polyubiquitin chains of RIP1 then serve as scaffolds to facilitate the recruitment of TAK1/TAB1/TAB2 and IKK-α/IKK-β/NEMO complexes, leading to TAK1 activation and TAK1-mediated activation of the IKK complex. Consequently, activated IKK phosphorylates the cytoplasmic IκBs, which triggers K48-linked polyubiquitination and proteasomal degradation of IκBs, thus allowing NF-κB to translocate into the nucleus and

*These two authors contributed equally to this work.
Correspondence: Jun Li
Tel: +86-20-87335828; Fax: +86-20-87335828
E-mail: lijun37@mail.sysu.edu.cn
Received 1 March 2012; revised 10 July 2012; accepted 25 September 2012; published online 18 December 2012

activate stimulus-specific gene programs [1, 2, 11-13]. Recently, it has been reported that linear ubiquitination of NEMO and unanchored polyubiquitin chains are also involved in NF-κB activation [14, 15].

On the other hand, ubiquitin deconjugation is mediated by multiple deubiquitinating enzymes, such as CYLD, A20 and cellular zinc finger anti-NF-κB (Cezanne), which serve as negative regulators in NF-κB signaling [4, 16]. CYLD, a K63-specific deubiquitinase, has been demonstrated to inhibit the NF-κB signal transmission by specifically deconjugating the K63-linked polyubiquitin chains from multiple intermediaries of the NF-κB signaling pathway, such as TRAF2, TRAF6, RIP1, NEMO and BCL3 [17-21]. However, A20, functioning as an ubiquitin-editing enzyme, negatively regulates NF-κB signaling through dual mechanisms, i.e. deconjugation of K63-linked polyubiquitin chains from RIP1 and subsequent conjugation of RIP1 with K48-linked polyubiquitin chains for proteasomal degradation. A20 can also dismantle K63-linked polyubiquitin chains from TRAF2, TRAF6 and NEMO, which results in suppression of NF-κB signaling [3, 22, 23]. Cezanne, a newly identified member of the A20 family of deubiquitinases, was reported to switch off the NF-κB pathway by deconjugating K63-polyubiquitin chains from RIP1 and TRAF6 [24, 25].

MicroRNAs (miRNAs), a class of non-coding RNAs, function as negative gene regulators. Through binding with partially complementary sequences in the 3′-untranslated regions (3′-UTR) of targeted mRNAs, individual miRNAs can simultaneously regulate a variety of target genes, potentiating their function at multiple levels in development and progression of human cancers [26, 27].

Previously, through microarray profiling, we found miR-486 to be one of most substantially overexpressed miRNAs in human primary glioma tissues of varying WHO grades [28]. Herein, we report that miR-486 sustains the NF-κB signaling pathway via directly repressing multiple NF-κB-negative regulators, including Cezanne, CYLD, ITCH, TNIP1, TNIP2 and TNIP3. Furthermore, we show that miR-486 overexpression results in an aggressive phenotype of glioma cells both *in vitro* and *in vivo*. Taken together, our findings demonstrate that miR-486 functions as an oncogenic miRNA in gliomas by conferring constitutive activation of the NF-κB signaling pathway.

Results

Cezanne reduction is associated with progression of gliomas

Cezanne, a newly identified member of the A20 family of deubiquitinases, functions as a negative feedback regulator of the NF-κB pathway under physiological conditions [24, 25], which suggests that it may have roles in inhibition of cancer progression. As expected, we found that the expression of Cezanne protein was differentially reduced in all 8 primary glioma tissues compared with the paired tumor-adjacent brain tissues, and in all 14 tested glioma cell lines compared with primary normal human astrocytes (NHA) (Figure 1A and 1B). These results indicate that Cezanne is downregulated in gliomas. Furthermore, Cezanne expression was analyzed in 169 paraffin-embedded, archived glioma specimens. Statistical analysis revealed that Cezanne expression correlated inversely with the glioma WHO grading and positively with patient survival time ($P < 0.001$; $P < 0.001$; Supplementary information, Tables S1, S2 and Figure 1C). These results suggest a possible link between Cezanne reduction and progression of human gliomas.

To investigate the effect of Cezanne reduction on glioma progression, we employed a knockdown cell model, which was created using Cezanne-specific shRNAs (Supplementary information, Figure S1A). As shown in Supplementary information, Figure S1B and S1C, Cezanne-silenced glioma cells exhibited higher growth rates and anchorage-independent growth abilities, compared to control cells. Meanwhile, we observed that silencing Cezanne also enhanced the invasive ability of glioma cells and the ability of glioma cells to induce human umbilical vein endothelial cells (HUVEC) tubule formation (Supplementary information, Figure S1D and S1E). Furthermore, we established U87MG and SNB19 glioma cell lines stably overexpressing Cezanne and implanted them into mouse brains. As shown in Figure 1D, tumors formed by Cezanne-overexpressing glioma cells showed dramatically decreased microvascular density (MVD) levels, as indicated by a reduction of CD31 signals, as well as a lower proliferation index and higher percentage of TUNEL-positive tumor cells as compared with control tumors. Importantly, supershift analysis in an electrophoretic mobility shift assay (EMSA) revealed that the NF-κB activities and the binding ability of NF-κB dimer with DNA in the Cezanne-overexpressing tumors dramatically decreased compared with those in control tumors (Supplementary information, Figure S2). These results further support the notion that Cezanne functions as a tumor suppressor in gliomas and inhibits NF-κB activity *in vivo*.

miR-486 targets and suppresses Cezanne

To better understand the mechanism by which Cezanne is reduced in gliomas, its mRNA expression levels were examined. Consistent with the data shown in

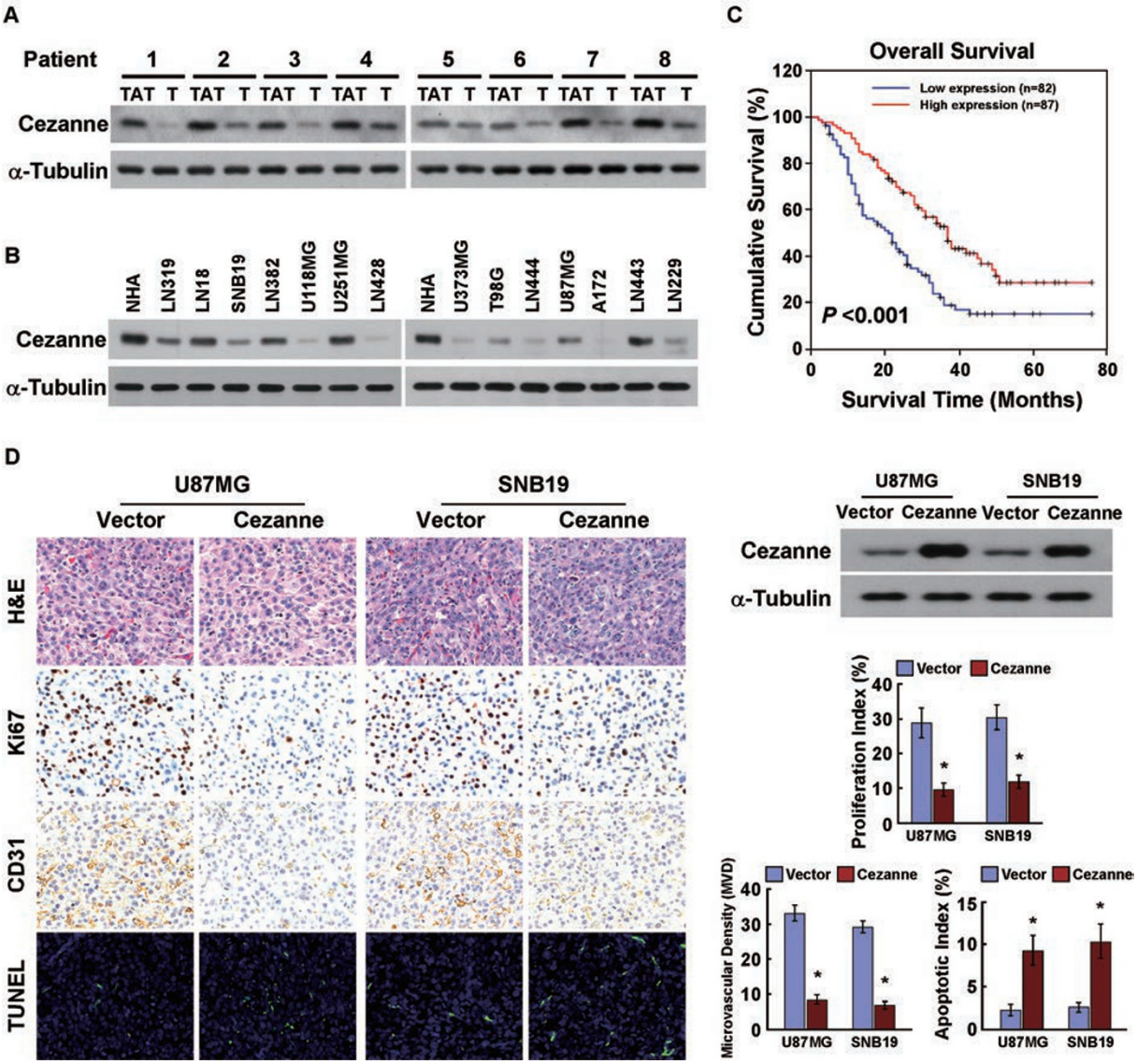

Figure 1 Cezanne reduction is associated with progression of gliomas. **(A**, **B)** Western blotting analysis of Cezanne expression in 8 paired primary glioma tissues (T) and tumor-adjacent tissues (TAT) **(A)**, and in NHA and 14 glioma cell lines **(B)**. α-Tubulin served as the loading control. **(C)** Kaplan-Meier analysis of Cezanne levels in WHO grade I-IV gliomas and survival of patients ($P < 0.001$, log-rank test). **(D)** Re-constitution of Cezanne inhibited glioma progression *in vivo*. Vector- or Cezanne-transduced U87MG and SNB19 glioma cells were stereotactically implanted into the brains of mice. Left panel: paraffin-embedded tumor sections were stained with H&E or immunostained with Ki67 or CD31. Apoptotic cells were visualized by TUNEL staining (green) and counterstained with DAPI (blue). Original magnification, ×200. Upper-right panel: western blotting analysis of Cezanne in vector- or Cezanne-transduced U87MG and SNB19 glioma cells. Lower-right panel: quantification of the proliferation index, MVD and apoptotic index in tumor sections. Each bar represents the mean ± SD of three independent experiments. *$P < 0.05$.

published microarrays (NCBI/GEO/GSE4290; $n = 180$, including 23 non-tumor and 157 tumor samples), our real-time PCR analysis revealed no significant alteration of *Cezanne* mRNA levels in eight glioma tissues compared with those in paired tumor-adjacent brain tissues (Supplementary information, Figure S3A and S3B), suggesting that Cezanne reduction in gliomas is regulated at the post-transcriptional level.

Analysis using publicly available algorithms (TargetScan, Pictar, miRANDA) showed that Cezanne is the predicted target of miR-486 (Figure 2A), a miRNA that has been found to be substantially overexpressed in

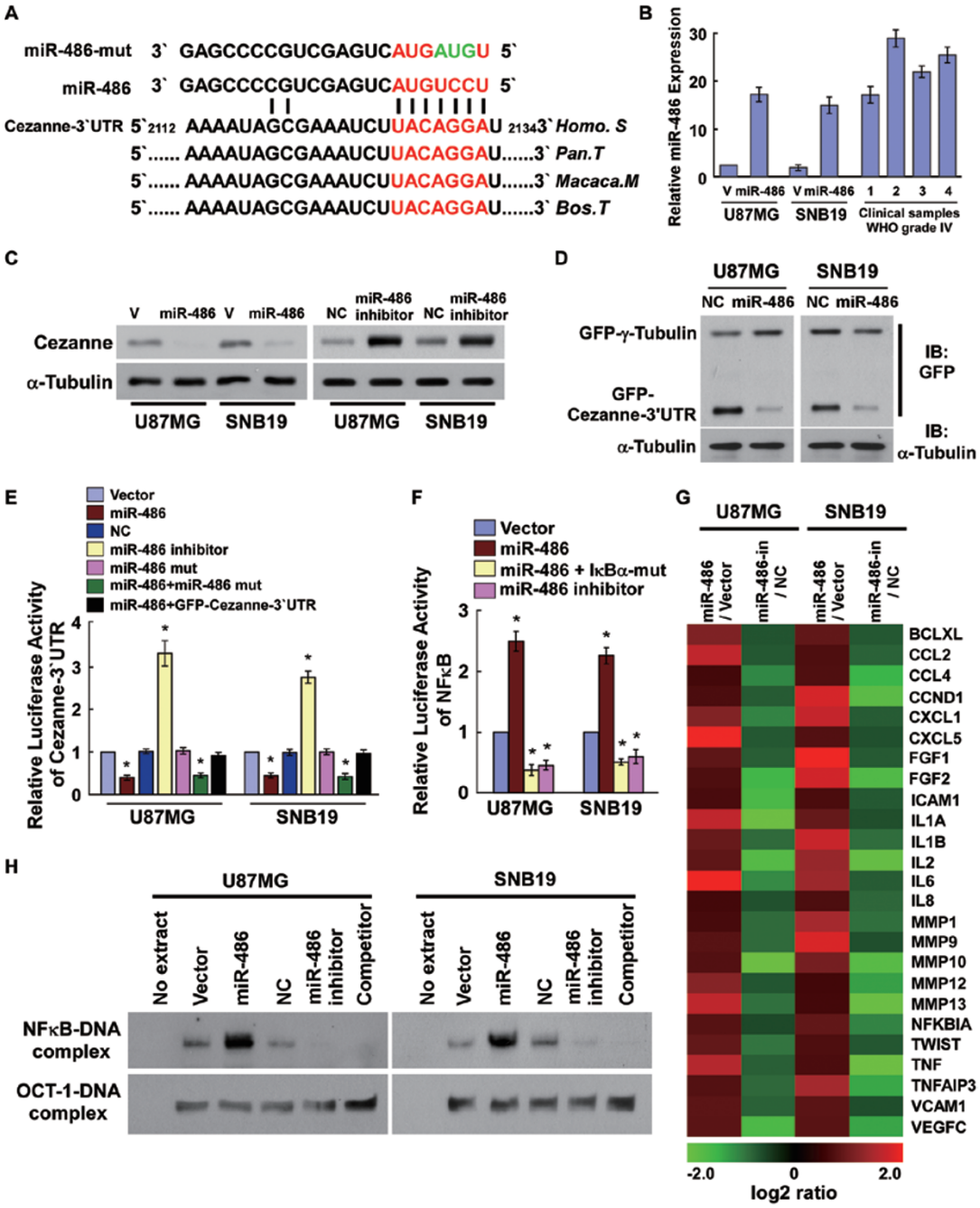

Figure 2 miR-486 directly targets cezanne and activates NF-κB signaling. **(A)** Predicted miR-486 target sequence in the 3′UTR of Cezanne (Cezanne-3′UTR) and mutant containing three altered nucleotides in the seed sequence of miR-486 (miR-486-mut). **(B)** Real-time PCR analysis of miR-486 expression in the indicated cells and 4 WHO grade IV glioma samples, compared with that in U87MG cells. Transcript levels were normalized by *U6* expression. **(C)** Western blotting analysis of Cezanne expression in vector- or miR-486-transduced cells, or in cells transfected with negative control (NC) or miR-486 inhibitor. α-Tubulin served as the loading control. **(D)** Western blotting analysis of GFP expression in the indicated cells. **(E)** Luciferase activity of Cezanne-3′UTR in vector- or miR-486-transduced cells; miR-486-transduced cells transfected with miR-486-mut or GFP-Cezanne-3′UTR; or vector-transduced cells transfected with NC or miR-486 inhibitor. **(F)** Luciferase-reported NF-κB activity in the indicated cells. **(G)** Real-time PCR analysis showed an apparent overlap between NF-κB-dependent and miR-486-regulated gene sets. The pseudocolor represents the intensity scale of miR-486 versus vector, or miR-486 inhibitor versus NC, generated by a log2 transformation. **(H)** EMSA showed that the endogenous NF-κB activity dramatically increased in miR-486-transduced cells but decreased in miR-486-inhibited cells. OCT-1 DNA-binding complexes served as a control. Each bar represents the mean ± SD of three independent experiments. **P* < 0.05.

gliomas [28]. To investigate the effect of miR-486 on Cezanne expression and its biological role in gliomas progression, U87MG and SNB19 glioma cells were engineered to stably overexpress miR-486 (Figure 2B). Immunoblotting analysis revealed that the expression of Cezanne was decreased in miR-486-transduced cells and increased in miR-486 inhibitor-transfected cells compared with control cells (Figure 2C). Interestingly, ectopically expressing miR-486 had no effect on GFP-γ-tubulin expression but dramatically decreased the expression of GFP containing the 3′-UTR of Cezanne, suggesting that miR-486 specifically targets the 3′-UTR of Cezanne (Figure 2D). Furthermore, results of the luciferase reporter assay showed that miR-486 overexpression decreased and miR-486 inhibition increased the luciferase activity of the Cezanne 3′-UTR (Figure 2E), whereas the miR-486 mutant failed to show an inhibitory effect on the luciferase expression (Figure 2E). Collectively, our data demonstrate that Cezanne is a *bona fide* target of miR-486.

miR-486 activates NF-κB signaling

As Cezanne has been reported to play a role in inhibition of NF-κB activity [24, 25], we then examined the effect of miR-486 on NF-κB activation. As shown in Figure 2F and 2G, the luciferase activity of the NF-κB reporter and numerous well-known NF-κB downstream target genes significantly increased in miR-486-transduced cells and decreased in miR-486-inhibited cells, suggesting that miR-486 contributes to NF-κB activation. In contrast, the stimulatory effect of miR-486 on NF-κB activation was drastically inhibited in response to the transfected IκBα dominant-negative mutant (IκBα-mut) (Figure 2F). Concordantly, results of the EMSA assay showed that miR-486 overexpression increased, while its inhibition decreased, the endogenous NF-κB activity in both U87MG and SNB19 glioma cells (Figure 2H), further demonstrating an important role of miR-486 in NF-κB activation.

miR-486 directly suppresses multiple NF-κB negative regulatory genes

However, re-introduction of the Cezanne ORF (without 3′UTR) into miR-486-transduced cells only partially abrogated miR-486-induced NF-κB activation (Figure 3A), implying that, in addition to Cezanne, other targets of miR-486 may also be involved in NF-κB activation. Interestingly, we found that CYLD, ITCH, TNIP1, TNIP2 and TNIP3, the reported NF-κB-negative regulators [20, 29, 30], were also the potential targets of miR-486 (Figure 3B, left panel). Indeed, immunoblotting analysis showed that overexpression of miR-486 repressed, while inhibition of miR-486 increased, the expression levels of CYLD, ITCH, TNIP1, TNIP2 and TNIP3 (Figure 3B, right panel). Furthermore, the luciferase activity and miRNP immunoprecipitation assays demonstrated that miR-486 could directly associate with the 3′-UTR of their transcripts (Figure 3C-3D and Supplementary information, Figure S4A). Moreover, we found that miR-486 dysregulation did not affect the expression of TRAF5, TRAF6, IKK-α, IKK-β and IKK-γ in the glioma cells (Supplementary information, Figure S4B). However, the expression levels of A20, c-IAP2 and XIAP, the downstream targets of NF-κB, were increased in miR-486-transduced glioma cells. Blocking NF-κB pathway by overexpressing IκBα-mut abolished the effect of miR-486 on A20 upregulation (Supplementary information, Figure S4B and S4C). Thus, these results further demonstrate that miR-486 activates the NF-κB pathway through direct suppression of NF-κB-negative regulators.

miR-486 promotes ubiquitin conjugation in NF-κB signaling and sustains NF-κB activity

Since the effects of these miR-486 targets on NF-κB deactivation are associated with ubiquitin deconjugation of NF-κB cascades, we then examined the impact of miR-486 on the ubiquitination status of NF-κB signaling intermediaries. As shown in Figure 4A, miR-486 overexpression drastically increased, but its inhibition decreased, the K63-polyubiquitin levels of RIP1 and NEMO in glioma cells. Concordantly, the phosphorylation level of IKK-β was significantly induced in miR-486-overexpressing cells but reduced in miR-486-inhibited cells (Figure 4B), indicating that miR-486 enhances IKK activity. Furthermore, we also observed that the duration of decrease in IκBα level and endogenous NF-κB DNA-binding activity after TNF-α treatment were significantly prolonged in miR-486-transduced cells but the reverse was true in miR-486 inhibitor-transfected cells (Figure 4C and 4D), suggesting that miR-486 overexpression sustains NF-κB activity in glioma cells.

miR-486 overexpression correlates with progression of human gliomas

Our previous microarray analysis showed that miR-486 is substantially overexpressed in gliomas [28]. Consistently, real-time PCR analysis revealed that miR-486 was markedly overexpressed in 8 primary glioma tissues compared with the paired tumor-adjacent brain tissues, as well as in all 14 tested glioma cell lines compared with NHA (Figure 5A and 5B). To assess whether miR-486 overexpression is linked to glioma progression, we further analyzed miR-486 levels in 169 archived clinical glioma specimens. As shown in Figure 5C, miR-486 lev-

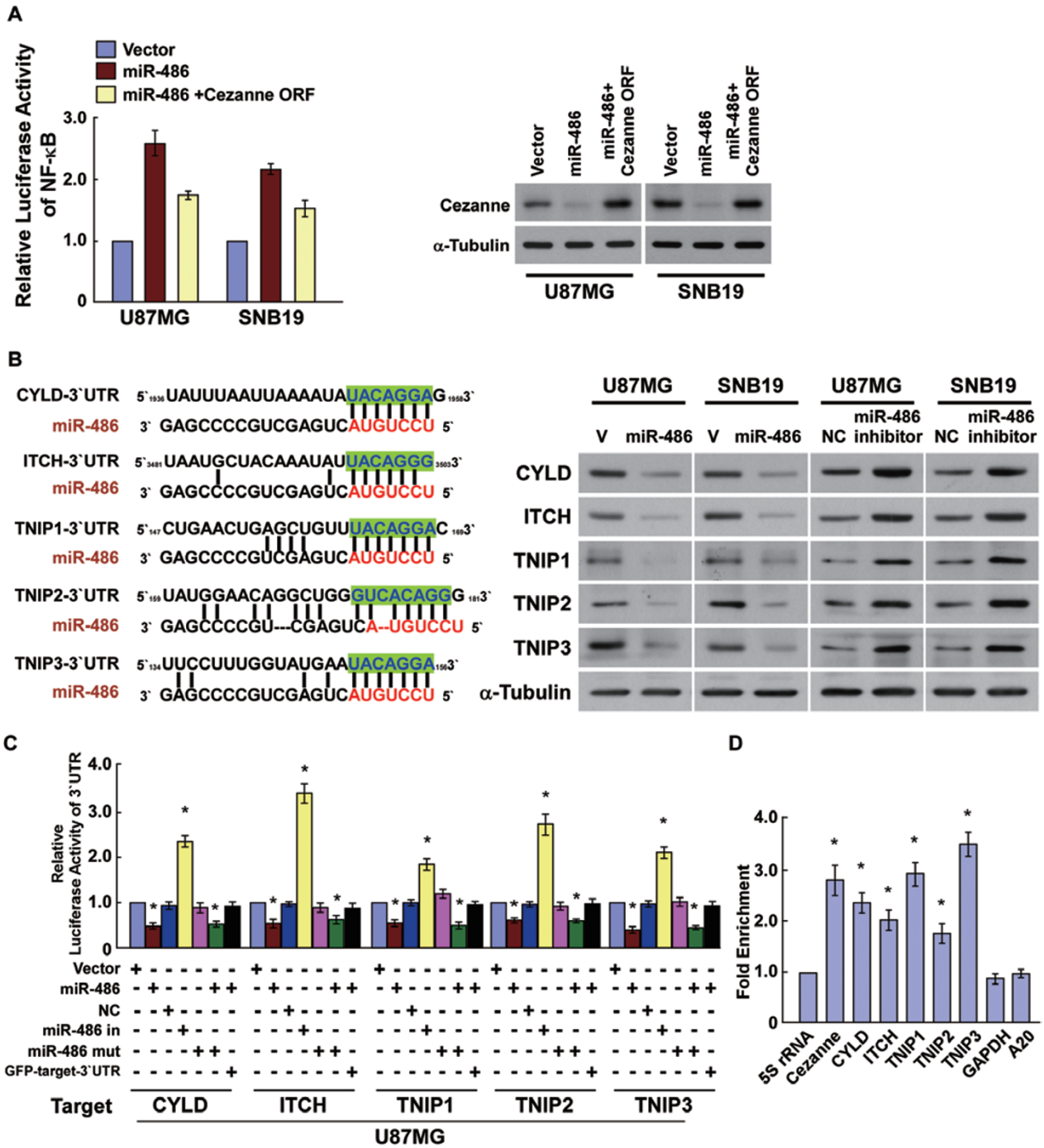

Figure 3 miR-486 represses multiple NF-κB-negative regulators. **(A)** Luciferase reporter NF-κB activity (left panel) and Cezanne expression (right panel) in the indicated cells. Recovery of Cezanne expression in miR-486-transduced cells comparable to that in control cells, via transfection with Cezanne ORF (without 3′UTR), only partially inhibited miR-486-induced NF-κB activity. **(B)** Predicted miR-486 target sequences in CYLD-3′UTR, ITCH-3′UTR, TNIP1-3′UTR, TNIP2-3′UTR and TNIP3-3′UTR (left panel) and the expression of CYLD, ITCH, TNIP1, TNIP2 and TNIP3 in the indicated cells analyzed by western blotting (right panel). α-Tubulin served as the loading control. **(C)** Luciferase activities of CYLD-3′UTR, ITCH-3′UTR, TNIP1-3′UTR, TNIP2-3′UTR or TNIP3-3′UTR in vector- or miR-486-transduced cells, or in miR-486-transduced cells transfected with miR-486-mut or GFP-(CYLD, ITCH, TNIP1, TNIP2 or TNIP3)-3′UTR, or in vector-transduced cells transfected with NC or miR-486 inhibitor. **(D)** miRNP immunoprecipitation assay showed association of miR-486 with *Cezanne, CYLD, TNIP1, TNIP2, TNIP3* and *ITCH*. *GAPDH* and *A20* served as negative controls. Expression levels were normalized by *5S rRNA*. Each bar represents the mean ± SD of three independent experiments. **P* < 0.05.

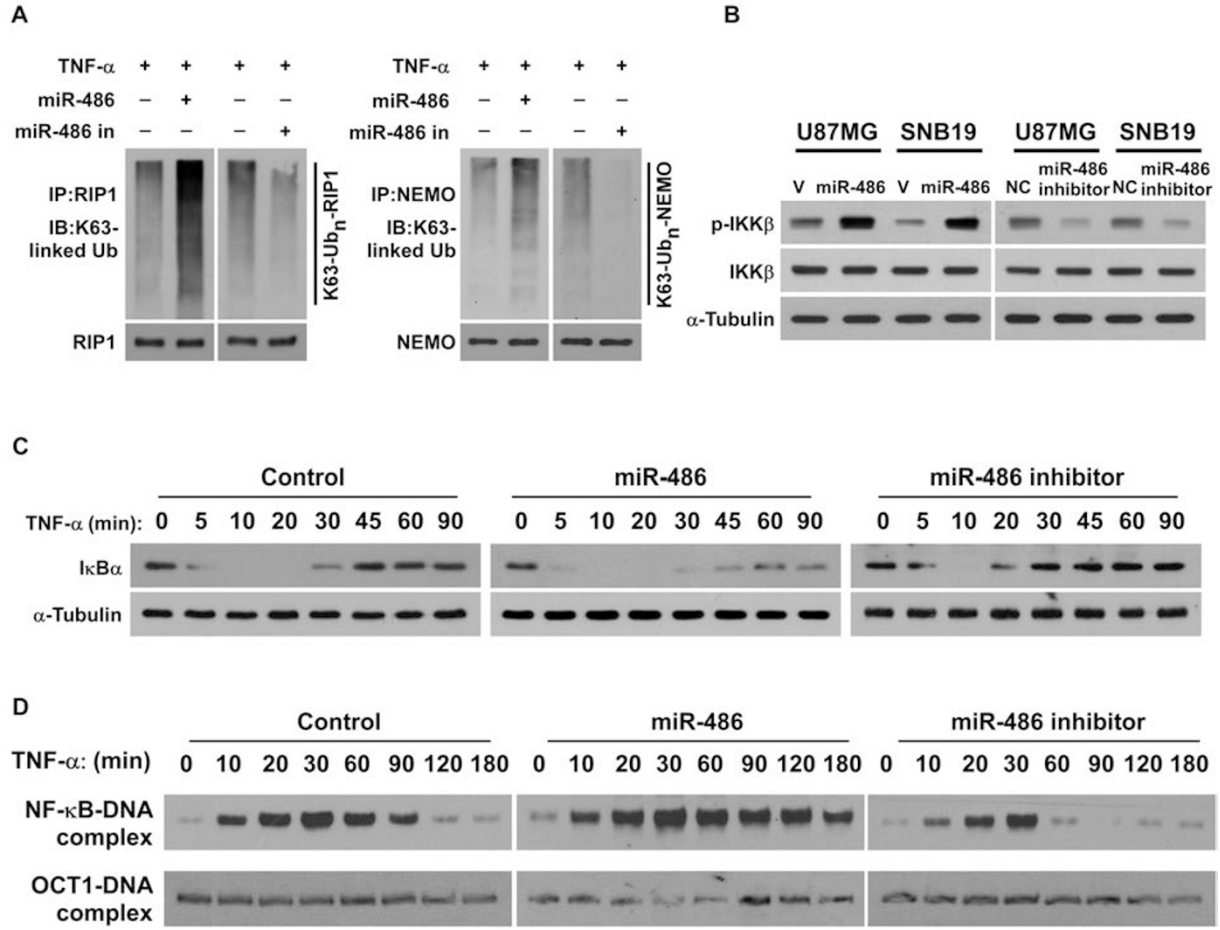

Figure 4 miR-486 sustains NF-κB activity. **(A)** Western blotting analysis of the endogenous K63-linked polyubiquitin levels of RIP1 (left panel) and NEMO (right panel) in the indicated cells treated with TNF-α (10 ng/ml). **(B)** Western blotting analysis of phospho-IKK-β and total IKK-β expression in the indicated cells treated with TNF-α (10 ng/ml). **(C)** Western blotting analysis of IκBα expression in the indicated cells treated with TNF-α (10 ng/ml). α-Tubulin was used as a loading control. **(D)** EMSA analysis of NF-κB activity in the indicated cells treated with TNF-α (10 ng/ml) for the indicated times.

els remained low in grade I tumors but became markedly higher in those at grade III and was further elevated in grade IV tumors. Statistical analysis revealed that miR-486 levels strongly correlated with glioma WHO grade and inversely with patient survival ($P < 0.001$; $P < 0.001$) (Figure 5D, Supplementary information, Tables S3 and S4), suggesting that miR-486 plays important roles in glioma progression and that its levels are associated with poor overall survival in patients with gliomas.

Upregulation of miR-486 augments glioma aggressiveness in vitro and in vivo

We then evaluated the biological role of miR-486 overexpression in glioma progression. As shown in Figure 6A and 6B, miR-486 overexpression dramatically increased, while miR-486 suppression reduced, the anchorage-independent growth abilities and the invasiveness of both U87MG and SNB19 glioma cells. Meanwhile, we observed that miR-486 overexpression strongly provoked, while its inhibition abrogated, the ability of glioma cells to induce the formation of vessels in chicken chorioallantoic membranes (CAM, Figure 6C). Consistently, silencing miR-486 in U87MG and SNB19 glioma cells, using cholesterol-conjugated 2′-O-Me antagomir-486, also significantly increased the luciferase activities of the 3′UTR of Cezanne, CYLD, ITCH and TNIP1-3, decreased the luciferase reporter NF-κB activity, reduced invasiveness of glioma cells and decreased the ability of glioma cells to induce HUVEC tube formation (Supplementary information, Figure S5A-S5E). Thus, these results further support the view that miR-486 overexpression is linked with progression of

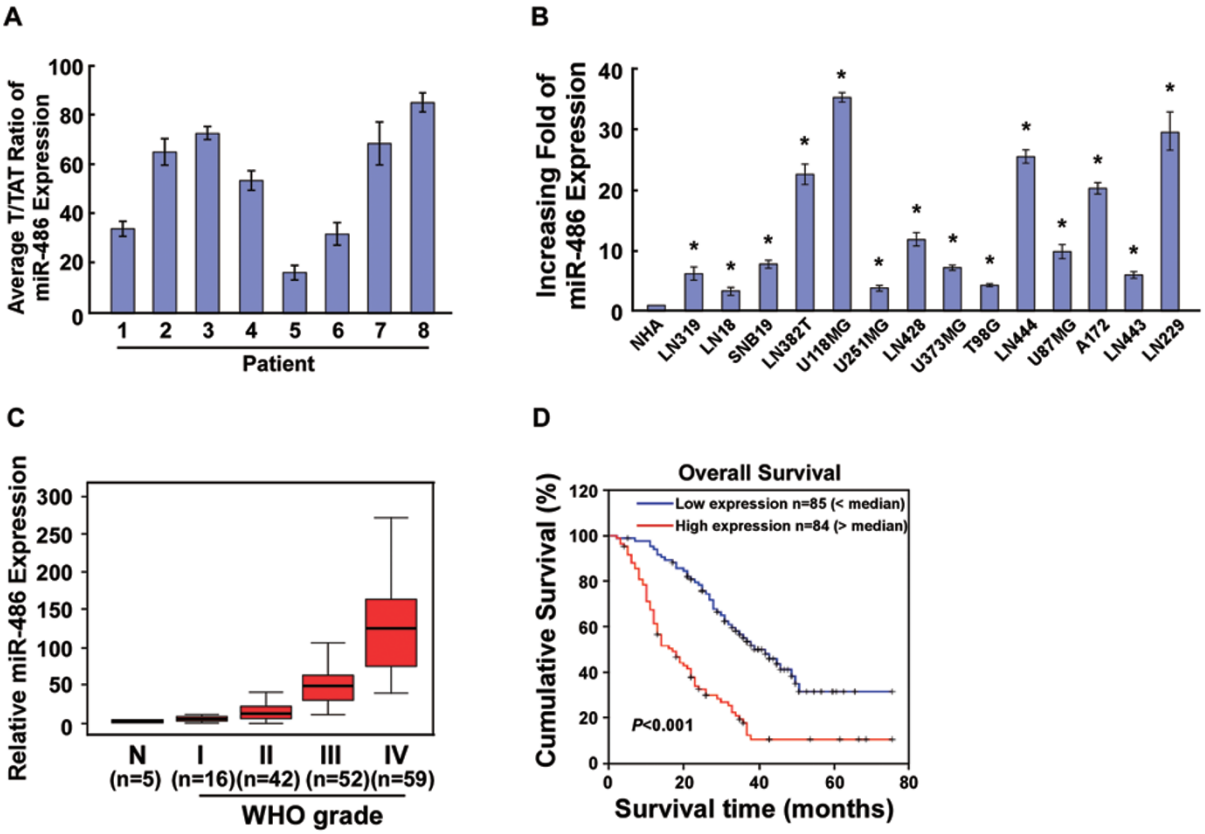

Figure 5 miR-486 is overexpressed in gliomas. **(A**, **B)** Real-time PCR analysis of miR-486 expression in 8 paired primary glioma tissues (T) and tumor-adjacent tissues (TAT) **(A)**, as well as in NHA and the indicated 14 glioma cell lines **(B)**. Transcript levels were normalized by *U6* expression. **(C)** Correlation between miR-486 expression in normal brain tissues and WHO grading of gliomas assessed by real-time PCR. Transcript levels were normalized by *U6* expression. The boundaries of the boxes represent the lower and upper quartiles; lines within boxes and whiskers denote median and extremum, respectively. **(D)** Correlation between miR-486 levels and survival by Kaplan-Meier analysis of patients with low (< the median, n = 85) or high (> the median, n = 84) miR-486 expression. Each bar represents the mean ± SD of three independent experiments. *P < 0.05.

gliomas. Importantly, blocking the NF-κB pathway by ectopically expressing IκBα-mut drastically reduced the stimulatory effect of miR-486 on invasiveness, proliferation and angiogenesis of glioma cells (Figure 6A-6C), demonstrating that functional NF-κB activation is vital to miR-486-induced aggressiveness of glioma cells.

The oncogenic role of miR-486 in promoting aggressiveness of gliomas was further examined *in vivo* by stereotactic implantation of tumor cells into brains of nude mice. We employed a stable miRNA sponge strategy to inhibit miR-486 *in vivo*. As shown in Figure 6D, miR-486-overexpressing tumors exhibited higher Ki67 signals, increased MVD and fewer TUNEL-positive tumor cells compared with control tumors. By contrast, the Ki67 and CD31 signals dramatically decreased, while the number of TUNEL-positive cells increased, in miR-486-inhibited tumors. Strikingly, borders of the tumors formed by U87MG/miR-486 cells displayed interspersed fibroblast-like structures that had invaded into the surrounding normal brain tissue, in contrast to the control tumor, which showed sharp edges that expanded as spheroids, indicating that miR-486 overexpression enhances the invasive ability of glioma cells *in vivo* (Figure 6D). Furthermore, immunohistochemistry (IHC) analysis showed that the expression levels of MMP-9 and VEGF-C, two NF-κB downstream targets, were markedly elevated in miR-486-expressing tumors but decreased in miR-486-inhibited tumors (Figure 6D). Consistently, NF-κB activity in the miR-486-expressing tumors was higher, while it was lower in miR-486-inhibited tumors, compared with that in control tumors (Figure 6E), indicating that the miR-486-induced invasiveness and angiogenesis of glioma cells *in vivo* are highly relevant to NF-κB activation. More importantly, Kaplan-Meier

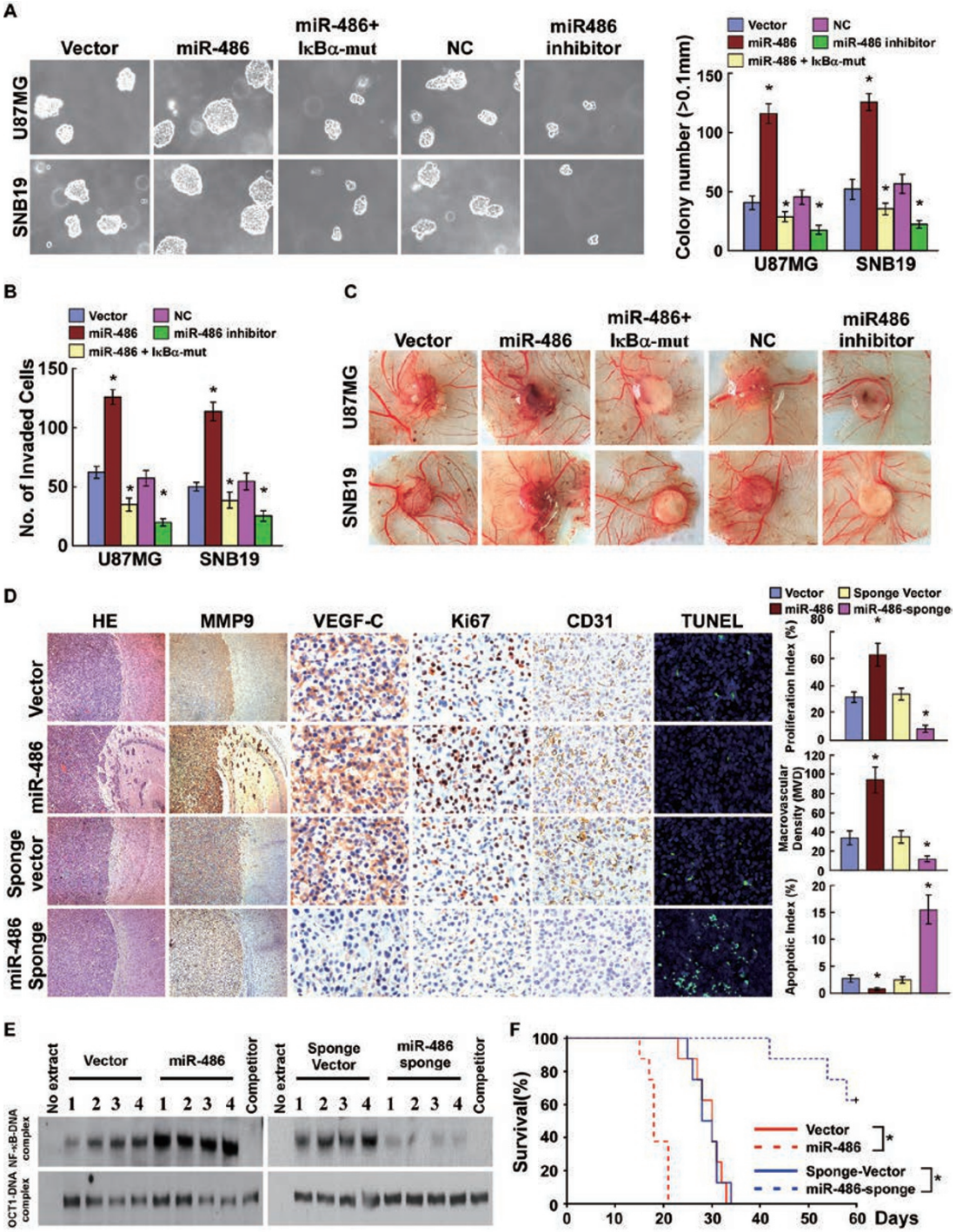

Figure 6 miR-486 promotes aggressive phenotype of glioma cells *in vitro* and *in vivo*. **(A)** Representative micrographs (left panel) and quantification (right panel) of colonies determined by anchorage-independent growth assays. **(B)** Quantification of the indicated invaded cells analyzed with a transwell matrix penetration assay. **(C)** Representative images of the CAM blood vessels stimulated with conditioned medium from the indicated cells. **(D)** H&E and IHC staining showed that overexpression of miR-486 induced, while suppression of miR-486 inhibited, the aggressive phenotype of glioma cells *in vivo*, as indicated by the expression of MMP-9, VEGF-C, Ki67, CD31 and TUNEL-positive cells and by the invaded glioma cells in surrounding normal brain. Original magnification, ×400. **(E)** EMSA of the endogenous NF-κB activity in four randomly selected U87MG/vector tumors and U87MG/miR-486 tumors (left panel), or U87MG/Sponge-vector tumors and U87MG/miR-486-sponge tumors (right panel). OCT-1 DNA-binding complexes served as a control. **(F)** Kaplan-Meier survival curve for the indicated mice (n = 8). Each bar represents the mean ± SD of three independent experiments. *P < 0.05.

analysis demonstrated that the mice bearing miR-486-overexpressing cells survived significantly shorter, but the mice bearing miR-486-inhibited cells survived much longer, than controls (Figure 6F). Taken together, these results demonstrate that miR-486 plays important roles in glioma progression.

miR-486 inhibition reduces NF-κB activity in patient-derived glioma cells (PDGCs)

It has been demonstrated that primary cultured cells from glioma biopsies show similar properties to cells present in the tumor mass [31]. Therefore, we further examined the effect of miR-486 inhibition on NF-κB activity in PDGCs. Consistent with the results obtained from glioma cell lines, inhibition or downregulation of miR-486 in PDGCs from two different patients significantly increased the luciferase activities of the 3′UTR of Cezanne, CYLD, ITCH, TNIP1, TNIP2 and TNIP3, but decreased the NF-κB-driven luciferase activity and endogenous NF-κB activity (Figure 7A-7C and Supplementary information, Figure S6A-S6E). The K63-polyubiquitin levels of endogenous RIP1 and NEMO induced by TNF-α were also dramatically decreased in the PDGCs transfected with the miR-486 inhibitor (Figure 7D). Furthermore, we observed that miR-486 inhibition significantly reduced the growth rate and invasiveness of PDGCs and decreased the ability of PDGCs to induce HUVEC tube formation (Figure 7E-7G). Therefore, our results demonstrate that suppression of miR-486 inhibits NF-κB activity and decreases the malignant properties of PDGCs.

Clinical relevance of miR-486/NF-κB pathway in human gliomas

Finally, we examined whether the miR-486/NF-κB signaling pathway identified by our study is clinically relevant. As shown in Figure 8A, correlation studies in 169 glioma specimens showed that the expression of p-IKK-β (S181) was strongly associated with miR-486 levels ($P < 0.001$). Furthermore, we found that miR-486 levels in 10 freshly collected glioma samples positively correlated with the mRNA levels of multiple NF-κB downstream targets, including *cyclin D1* ($r = 0.673$, $P = 0.033$), *MMP-9* ($r = 0.782$, $P = 0.008$), *VEGF-C* ($r = 0.745$, $P = 0.013$) and *Bcl-xL* ($r = 0.733$, $P = 0.016$), as well as DNA-binding activity of NF-κB ($r = 0.660$, $P = 0.038$) (Figure 8B), further supporting the concept that upregulation of miR-486 expression activates NF-κB signaling and results in glioma aggressiveness and poor clinical outcomes (Figure 9).

Discussion

Herein, we report that miR-486 sustains NF-κB signaling pathway by preventing deubiquitination of NF-κB signaling intermediaries. We demonstrate that miR-486 directly represses deubiquitinases, CYLD and Cezanne, and multiple A20 deubiquitinase activity modulators, including ITCH, TNIP-1, TNIP-2 and TNIP-3. Overexpression of miR-486 dramatically promotes glioma aggressiveness both *in vitro* and *in vivo* and inhibition of miR-486 leads to reduction of NF-κB activity and malignant properties of PDGCs. Importantly, the significant correlation detected between miR-486 levels with NF-κB hyperactivation was further confirmed in a cohort of human glioma samples. Hence, the miR-486/NF-κB pathway represents a critical mechanism for inducing constitutive NF-κB activation and promoting glioma aggressiveness.

Recently, gene expression profiling was employed to investigate the spectrum of genes differentially expressed in glioma cells and clinical specimens. Numerous candidate genes potentially involved in glioma development processes, such as proliferation, prevention of apoptosis, angiogenesis and invasion, have emerged. Assessing the function of these candidates has shown that components of the NF-κB pathway can serve as vital therapeutic targets for gliomas [32, 33]. Several molecular mechanisms for activation of NF-κB signaling have been proposed [1, 2, 7]. On the other hand, NF-κB signaling has also been found to be restricted by negative feedback mechanisms via induction of NF-κB inhibitors, IκBs and a number of NF-κB-negative regulators, such as A20, CYLD and Cezanne [4, 5]. However, how cancer cells simultaneously take priority over these feedback loops remains an enigma. Herein, we demonstrate that miR-486 sustains NF-κB activity via directly targeting and suppressing multiple NF-κB-negative regulators. Our findings not only present a novel mechanism by which multiple negative feedback loops are disrupted in cancer cells that result in constitutive NF-κB activation, but also support the concept that the NF-κB signaling pathway contributes to glioma progression.

Intense research efforts over the past decade have confirmed that the deubiquitinase A20 functions as a key negative regulator of NF-κB activation [3, 22, 23]. However, A20 expression was found to be elevated in gliomas. Overexpression of A20 in glioma cells confers resistance to TNF-α-induced cell death, and A20 knockdown resulted in reduction of the growth rates of glioma cells both *in vitro* and *in vivo*, indicating that A20 plays pro-tumorigenic roles in the development and progression of gliomas [34, 35]. How the negative regulatory effect of upregulated A20 on NF-κB signaling is disrupted in gliomas, however, remains unclear. Given that A20 does not have specificity for K63-linked polyubiquitin

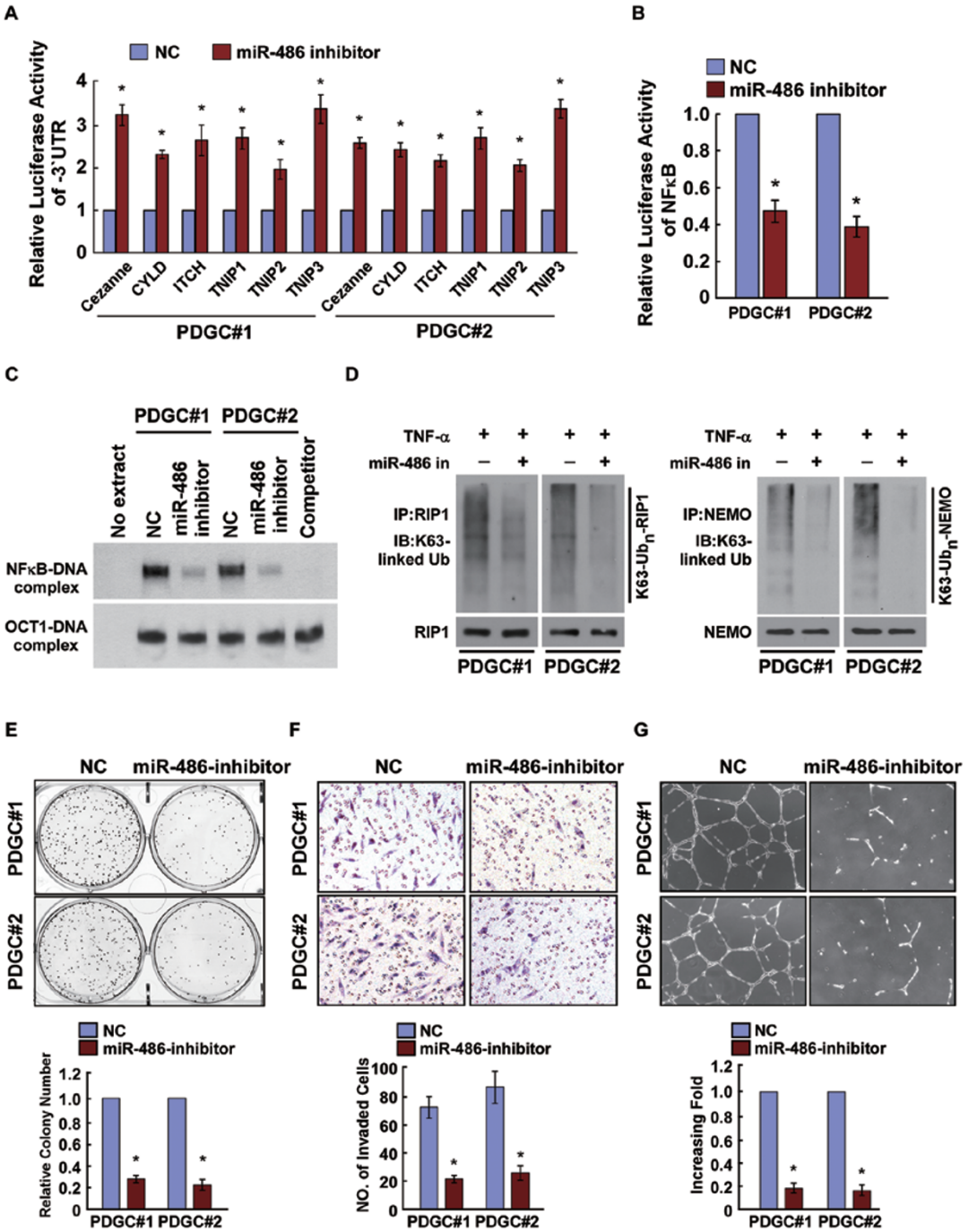

Figure 7 Suppression of miR-486 inhibits NF-κB and malignant properties of PDGCs. **(A)** Luciferase activities of Cezanne-3′UTR, CYLD-3′UTR, ITCH-3′UTR, TNIP1-3′UTR, TNIP2-3′UTR or TNIP3-3′UTR in PDGCs from two patients transfected with negative control (NC) or miR-486 inhibitor. **(B)** NF-κB reporter activities in PDGCs transfected with NC or miR-486 inhibitor. **(C)** EMSA showed the dramatically decreased endogenous NF-κB activity in PDGCs transfected miR-486 inhibitor, compared with that in NC-transfected PDGCs. Oct-1 DNA-binding complexes served as a control. **(D)** Western blotting analysis of the endogenous K63-linked polyubiquitin levels of RIP1 (left panel) and NEMO (right panel) in NC- or miR-486 inhibitor-transfected PDGCs treated with TNF-α (10 ng/ml). **(E)** Representative images (upper panel) and quantification (lower panel) of NC- or miR-486 inhibitor-transfected PDGCs analyzed in a clonogenic assay. **(F)** Representative images (upper panel) and quantification (lower panel) of invaded cells were analyzed in a transwell matrix penetration assay. **(G)** Representative images (upper panel) and quantification (lower panel) of HUVECs cultured on Matrigel-coated plates with conditioned medium from NC- or miR-486 inhibitor-transfected PDGCs. Each bar represents the mean ± SD of three independent experiments. *P < 0.05.

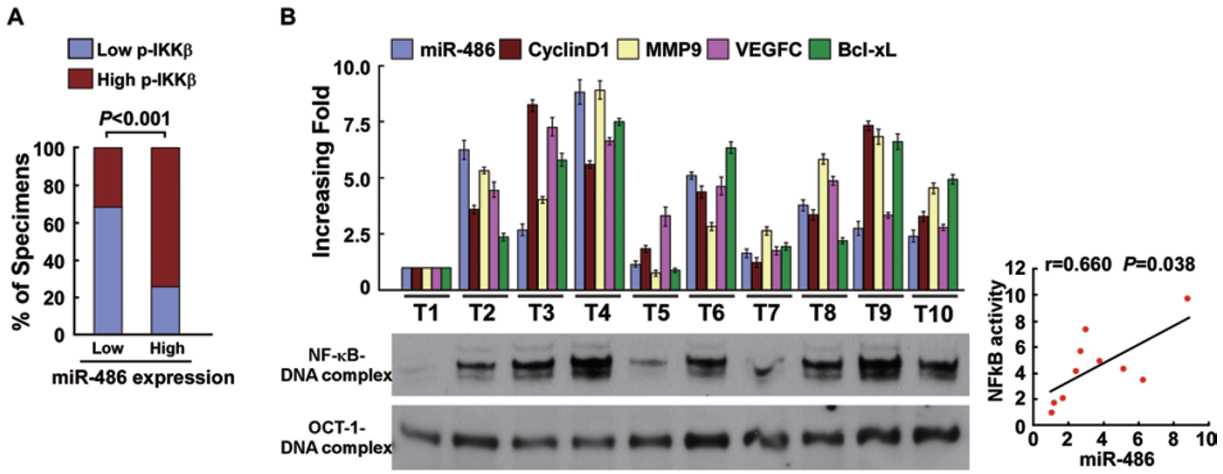

Figure 8 Clinical relevance of miR-486-induced NF-κB activation in human gliomas. **(A)** Percentages of specimens showing low or high p-IKK-β (S181) expression in relation to the expression levels of miR-486. **(B)** Analysis of expression (left) and correlation (right) of miR-486 with *MMP9*, *VEGF-C*, *Cyclin D1* and *Bcl-xL* mRNA expression, as well as activity of NF-κB in 10 freshly collected human glioma samples. Each bar represents the mean ± SD of three independent experiments.

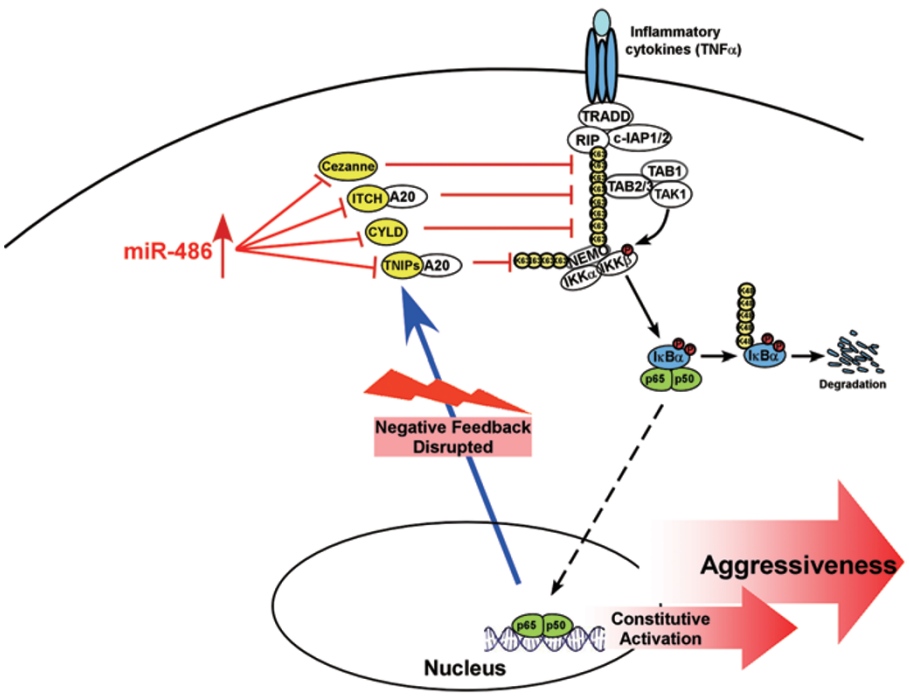

Figure 9 Model: miR-486 directly represses multiple NF-κB-negative regulators, resulting in disruption of NF-κB-negative feedback loops and constitutive activation of the NF-κB signaling pathway, ultimately leading to glioma aggressiveness and poor clinical outcomes for glioma patients.

chains but preferentially cleaves K48-linked polyubiquitin chains *in vitro*, A20 mediated-NF-κB inhibition may occur through cooperation with other proteins. Indeed, several A20-interacting proteins, such as TAX1BP1, RNF11, ITCH and TNIPs (also known as ABINs, including TNIP-1, TNIP-2 and TNIP-3) [29, 30, 36, 37], have been proposed to participate in the NF-κB inhibitory effect of A20 through modulation of A20 activity. For example, ITCH has been found to terminate NF-κB signaling by controlling A20-mediated recruitment and

inactivation of RIP1. TNIPs were found to be physically linked A20 to NEMO and promote A20-mediated NF-κB inhibition through deubiquitination of NEMO. Here, we demonstrate that miR-486 directly targets and suppresses the 3′UTR of *ITCH*, *TNIP1*, *TNIP2* and *TNIP3*, resulting in NF-κB activation. Therefore, our finding uncovers a miRNA-mediated mechanism by which the inhibition of NF-κB by upregulated A20 is interrupted in gliomas. Interestingly, we also found that overexpression of miR-486 increased, but inhibition of miR-486 decreased, the nuclear expression of p52 and the phosphorylation levels of MKK7 and JNK (Supplementary information, Figure S7A and S7B), suggesting that miR-486 might also contribute to modulation of non-canonical NF-κB and MAPK pathways [38, 39]. Apparently, the precise mechanisms by which miR-486 activates non-canonical NF-κB and MAPK pathways in gliomas need to be further investigated.

Over the past decade, deubiquitinases, such as A20 and CYLD, acting as key negative regulators of NF-κB signaling, have been characterized as tumor suppressors, and their deficiencies lead to increased susceptibility to tumor induction [20]. As a newly identified member of the A20 family of deubiquitinating enzymes, Cezanne acts as a feedback loop inhibitor of NF-κB signaling [24, 25]. However, its clinical significance and biological role in cancer remain largely unknown. In the current study, both clinical and experimental data suggest that Cezanne is a novel deubiquitinase-associated tumor suppressor in gliomas. We found that Cezanne expression was reduced in a large cohort of glioma specimens and that Cezanne levels correlated inversely with glioma WHO grading and positively with patient survival time. Restoration of Cezanne could significantly inhibit the progression of gliomas *in vivo*. Thus, our results not only suggest that Cezanne functions as a tumor suppressor in gliomas but also further support the notion that dysregulation of ubiquitin conjugation/deconjugation is involved in human cancer. Although Cezanne was reported to inhibit NF-κB signaling through removing K63-linked polyubiquitin chains from RIP1 [24, 25], Bremm *et al.* [40] found that Cezanne preferentially hydrolyzes K11-linked polyubiquitin chains. Interestingly, a recent study reported that K11-linked polyubiquitin chains of RIP1 can also serve as a platform for recruitment of NEMO and participate in TNF-α-stimulated NF-κB activation [41]. In this respect, investigating the selectivity of Cezanne for K11- or K63-linked ubiquitin chains may reveal a novel regulatory mechanism of NF-κB signaling and facilitate the discovery of new therapeutic targets for cancer treatment and prevention.

It has been reported that miR-486 is overexpressed in Sézary syndrome, K-ras mutated colorectal carcinoma and bronchioalveolar stem cells [42-44]. Importantly, Hu *et al.* [45] found that non-small cell lung cancer patients with high serum levels of miR-486 have shorter overall survival times. Consistently, we found that miR-486 expression significantly correlated with WHO glioma grading. Upregulation of miR-486 augmented glioma aggressiveness *in vitro* and *in vivo*, and inhibition of miR-486 reduced malignant properties of PDGCs. Thus, our results together with previous studies suggest that miR-486 plays important roles in the progression of gliomas and that miR-486 expression may be useful for evaluating responses to therapy and surveillance of cancer outcomes. Interestingly, Oh *et al.* [46] found that miR-486 is downregulated in gastric cancer and functions as a tumor suppressor. It has been proposed that a single miRNA may have several distinct functions in different cell types, which likely depends on the availability of specific targets or downstream effectors [47, 48]. The *miR-486* gene has been reported to be located in the intron of the *sAnk1* gene [49]. By analysis of the *sAnk1* promoter region using the CONSITE program, we found four typical TGF-β-responsive elements (SRE) and two tandem repeats of the TCF/LEF transcriptional responsive element, suggesting that the TGF-β/Smad and Wnt/β-catenin signalings may be involved in regulation of miR-486 expression. The mechanisms by which miR-486 is upregulated in gliomas are currently under investigation in our laboratory.

In summary, our study has revealed that miR-486 plays important roles in glioma progression and that miR-486 is a critical mediator involved in prolonged NF-κB activation. Given the common oncogenic roles of miR-486 and the NF-κB signaling pathway in human cancers, the current findings not only improve our understanding of the molecular mechanisms underlying NF-κB constitutive activation in cancer but also provide new insights into the development of therapeutic interventions for cancer via inhibition of miR-486.

Materials and Methods

Ethics statement

For the use of clinical materials for research purposes, prior patients' written consent and approval were obtained from the Sun Yat-sen University and Cancer Center Institutional Board. All animal studies were conducted with the approval of the Sun Yat-sen University Institutional Animal Care and Use Committee.

Tissue specimens and patient information

A total of 169 paraffin-embedded, archived glioma specimens and 8 freshly collected paired glioma tissues were histopathologically diagnosed at the First Affiliated Hospital of Sun Yat-sen

University from 2000 to 2010. All samples were collected and analyzed with prior written informed consent from the patients. Normal brain tissues were obtained from individuals who died in traffic accidents and confirmed to be free of any pre-existing pathologically detectable conditions. Prior donors' written consents and approvals from the Institutional Research Ethics Committee were obtained.

Cell lines and primary cultured tumor cells

Primary NHA were purchased from the Sciencell Research Laboratories (Carlsbad, CA, USA) and cultured according to the manufacturer's instruction. Glioma cell lines LN382T, A172, T98G, LN18, LN229, LN464, SNB19, U373MG, U87MG, LN444, LN443, LN428, U118MG, LN-Z308 and LN319 were from ATCC (Manassas, VA, USA), Drs E Van Meir (Emory University, USA) or Y-H Zhou (University of California, Irvin, CA, USA), respectively. These cells were grown in the Dulbecco's modified Eagle's medium supplemented with 10% fetal bovine serum. Fresh brain tumor tissues obtained from the First Affiliated Hospital of Sun Yat-sen University were collected and processed within 30 min after resection. The primary cultured tumor cells were obtained after mechanical dissociation according to a previously described technique [31].

Plasmids, virus production and infection of target cells

The human *miR-486* gene was PCR-amplified from genomic DNA and cloned into the pMSCV-puro retroviral vector (Supplementary information, Figure S8A). miR-486 sponge was constructed by annealing, purifying and cloning oligonucleotides containing six tandem "bulged" miR-486-binding motifs into pMSCV-vector (Supplementary information, Figure S8B). Human Cezanne was amplified by PCR from a human liver complementary DNA library (Clontech, Mountain View, CA, USA) and cloned into the pMSCV-vector. miR-486 inhibitor is a LNA/OMe-modified antisense oligonucleotide designed specifically to bind to and inhibit endogenous miR-486 molecule (Supplementary information, Figure S8C). Antagomir-486 is a cholesterol-conjugated 2′-O-Me-modified antisense oligonucleotide designed specifically to degrade endogenous miR-486 molecule (Supplementary information, Figure S8D). The 3′UTR regions of human Cezanne, CYLD, ITCH, TNIP1, TNIP2 and TNIP3, generated by PCR amplification from NHA, were cloned into the pGL3 luciferase reporter plasmid (Promega, Madison, WI, USA) and pGFP-C3 (Clontech). pBabe-Puro-IκBα-mut (plasmid 15291) expressing mutant IκBα was from Addgene (Cambridge, MA, USA). pNF-κB-luc and control plasmids (Clontech) was used to quantitatively examine NF-κB activity. Transfection of siRNAs or plasmids or miR-486 inhibitor or NC was performed using the Lipofectamine 2000 reagent (Invitrogen, Carlsbad, CA, USA) according to the manufacturer's instruction. Transfection efficiency was measured using FITC-labeled NC by flow cytometery for every experiment. Stable cell lines expressing miR-486 and miR-486 sponge were generated via retroviral infection using HEK293T cells, as has been previously described [50], and selected by treatment with 0.5 μg/ml puromycin beginning 48 h after infection for 10 days.

Western blotting

Western blotting was performed according to standard methods as described previously [51], using anti-CYLD, anti-TNIP1, anti-TNIP2, anti-TNIP3 antibodies (Sigma, Saint Louis, MI, USA); anti-IκBα, anti-p-IκBα, anti-p-IKK-β (Cell Signaling, Danvers, MA, USA) and anti-IKK-β antibodies (Santa Cruz Biotechnology, CA, USA); anti-ITCH, anti-Cezanne antibodies (Abcam, Cambridge, MA, USA). Blotting membranes were stripped and re-probed with anti-α-tubulin antibody (Sigma) as a loading control.

Immunohistochemistry

Immunohistochemical analysis was performed to study altered protein expression in 169 human glioma tissues. The procedure was carried out similarly to previously described methods [50]. The degree of immunostaining of formalin-fixed, paraffin-embedded sections was reviewed and scored independently by two observers, based on both the proportion of positively stained tumor cells and the intensity of staining. The proportion of tumor cells was scored as follows: 0 (no positive tumor cells), 1 (< 10% positive tumor cells), 2 (10-50% positive tumor cells) and 3 (> 50% positive tumor cells). The intensity of staining was graded according to the following criteria: 0 (no staining), 1 (weak staining = light yellow), 2 (moderate staining = yellow brown) and 3 (strong staining = brown). The staining index (SI) was calculated as staining intensity score × proportion of positive tumor cells. Using this method of assessment, we evaluated the indicated protein expression by determining the SI, scored as 0, 1, 2, 3, 4, 6 and 9. Cutoff values were chosen on the basis of a measure of heterogeneity with the log-rank test statistical analysis with respect to overall survival. The images were captured using the AxioVision Rel.4.6 computerized image analysis system (Carl Zeiss, Jena, Germany).

HUVEC tubule formation assay

HUVEC tubule formation and migration assay was performed as previously described [52]. Briefly, 200 μl Matrigel (BD Biosciences, Bedford, MA, USA) was pipetted into each well of a 24-well plate and polymerized for 30 min at 37 °C. HUVECs (2×10^4) in 200 μl of conditioned medium were added to each well and incubated at 37 °C, 5% CO_2 for 20 h. Pictures were taken under a 100× bright-field microscope, and the capillary tubes were quantified by measuring the total lengths of the completed tubule structure. Each condition was assessed at least in triplicate.

CAM assay

CAM assay was performed with of fertilized chicken eggs (day 6) using a method previously described [52]. A 1-cm diameter window was opened on the egg shell (Yueqin Breeding Co. Ltd, Guangdong, China). The surface of the dermic sheet on the floor of the air sac was removed to expose the CAM. A 0.5-cm diameter filter paper was first placed on top of the CAM, and 100 μl conditioned medium was added onto the center of the paper. After the window was closed with sterile adhesive tape, the eggs were incubated at 37 °C under 80-90% relative humidity for 4 days. Following fixation with stationary solution (methanol: acetone = 1:1) for 15 min, the CAMs were cut and harvested and gross photos of each CAM were taken with a digital camera (Panasonic, Osaka, Japan). The effect of conditioned media harvested from different cultured cells was evaluated by the number of second- and third-order vessels.

Intracranial brain tumor xenografts, IHC and hematoxylin

and eosin (H&E) staining

The indicated cells (5×10^5) were stereotactically implanted into individual nude mouse brains (n = 8/group). Whole brains removed from the sacrificed glioma-bearing mice were cut into 6 μm sections and subjected to IHC and H&E staining. After deparaffinization, sections were analyzed by IHC using an anti-Ki67, anti-MMP-9, anti-VEGF-C (Cell Signaling) or anti-CD31 antibody (Invitrogen) or H&E stained with Mayer's hematoxylin solution. The images were captured using the AxioVision Rel.4.6 computerized image analysis system (Carl Zeiss).

Statistical analysis

All statistical analyses were carried out using the SPSS 10.0 statistical software package. The chi-square test was used to analyze the relationships between Cezanne, miR-486 expression and clinicopathological characteristics. Bivariate correlations between study variables were calculated by Spearman's rank correlation coefficients. $P < 0.05$ in all cases was considered statistically significant.

Acknowledgments

This work was supported by Guangdong Province Universities and Colleges Pearl River Scholar Funded Scheme (GDUPS, 2012), Natural Science Foundation of China (81071780, 81030048, 91229101, U1201121, 81272196 and 81272198), the Science and Technology Department of Guangdong Province (S2011020002757 and S2012020010946) and the National Science and Technique Major Project (201005022-2).

References

1 DiDonato J, Mercurio F, Rosette C, *et al*. Mapping of the inducible IkappaB phosphorylation sites that signal its ubiquitination and degradation. *Mol Cell Biol* 1996; **16**:1295-1304.
2 Rodriguez MS, Wright J, Thompson J, *et al*. Identification of lysine residues required for signal-induced ubiquitination and degradation of I kappa B-alpha *in vivo*. *Oncogene* 1996; **12**:2425-2435.
3 Wertz IE, O'Rourke KM, Zhou H, *et al.* Deubiquitination and ubiquitin ligase domains of A20 downregulate NFkappaB signalling. *Nature* 2004; **430**:694-699.
4 Harhaj EW, Dixit VM. Deubiquitinases in the regulation of NF-κB signaling. *Cell Res* 2011; **21**:22-39.
5 Liu S, Chen ZJ. Expanding role of ubiquitination in NF-κB signaling. *Cell Res* 2011; **21**:6-21.
6 Skaug B, Jiang X, Chen ZJ. The role of ubiquitin in NF-kappaB regulatory pathways. *Annu Rev Biochem* 2009; **78**:769-796.
7 Wertz IE, Dixit VM. Signaling to NF-kappaB: regulation by ubiquitination. *Cold Spring Harb Perspect Biol* 2010; **2**:a003350.
8 Deng L, Wang C, Spencer E, *et al*. Activation of the IkappaB kinase complex by TRAF6 requires a dimeric ubiquitin-conjugating enzyme complex and a unique polyubiquitin chain. *Cell* 2000; **103**:351-361.
9 Wang C, Deng L, Hong M, Akkaraju GR, Inoue J, Chen ZJ. TAK1 is a ubiquitin-dependent kinase of MKK and IKK. *Nature* 2001; **412**:346-351.
10 Ea CK, Deng L, Xia ZP, Pineda G, Chen ZJ. Activation of IKK by TNFalpha requires site-specific ubiquitination of RIP1 and polyubiquitin binding by NEMO. *Mol Cell* 2006; **22**:245-257.
11 Chen ZJ, Parent L, Maniatis T. Site-specific phosphorylation of IκBα by a novel ubiquitination-dependent protein kinase activity. *Cell* 1996; **84**:853-862.
12 Ghosh S, Baltimore D. Activation *in vitro* of NFκB "by phosphorylation of its inhibitor IκB". *Nature* 1990; **344**:678-682.
13 Kanayama A, Seth RB, Sun L, *et al*. TAB2 and TAB3 activate the NF-κB pathway through binding to polyubiquitin chains. *Mol Cell* 2004; **15**:535-548.
14 Tokunaga F, Sakata S, Saeki Y, *et al*. Involvement of linear polyubiquitylation of NEMO in NF-kappaB activation. *Nat Cell Biol* 2009; **11**:123-132.
15 Xia ZP, Sun L, Chen X, *et al*. Direct activation of protein kinases by unanchored polyubiquitin chains. *Nature* 2009; **461**:114-119.
16 Düwel M, Hadian K, Krappmann D. Ubiquitin Conjugation and Deconjugation in NFκB Signaling. *Subcell Biochem* 2010; **54**:88-99.
17 Bignell GR, Warren W, Seal S, *et al*. Identification of the familial cylindromatosis tumour-suppressor gene. *Nat Genet* 2000; **25**:160-165.
18 Brummelkamp TR, Nijman SM, Dirac AM, Bernards R. Loss of the cylindromatosis tumour suppressor inhibits apoptosis by activating NFκB. *Nature* 2003; **424**:797-801.
19 Kovalenko A, Chable-Bessia C, Cantarella G, Israël A, Wallach D, Courtois G. The tumour suppressor CYLD negatively regulates NFκB signaling by deubiquitination. *Nature* 2003; **424**:801-805.
20 Sun SC. CYLD: a tumor suppressor deubiquitinase regulating NFkappaB activation and diverse biological processes. *Cell Death Differ* 2010; **17**:25-34.
21 Trompouki E, Hatzivassiliou E, Tsichritzis T, Farmer H, Ashworth A, Mosialos G. CYLD is a deubiquitinating enzyme that negatively regulates NFκB activation by TNFR family members. *Nature* 2003; **424**:793-796.
22 Lee EG, Boone DL, Chai S, *et al.* Failure to regulate TNF induced NFkB and cell death responses in A20-deficient mice. *Science* 2000; **289**:2350-2354.
23 Hymowitz SG, Wertz IE. A20: from ubiquitin editing to tumour suppression. *Nat Rev Cancer* 2010; **10**:332-341.
24 Enesa K, Zakkar M, Chaudhury H, *et al*. NF-κB suppression by the deubiquitinating enzyme Cezanne: a novel negative feedback loop in pro-inflammatory signaling. *J Biol Chem* 2008; **283**:7036-7045.
25 Evans PC, Taylor ER, Coadwell J, Heyninck K, Beyaert R, Kilshaw PJ. Isolation and characterization of two novel A20-like proteins. *Biochem J* 2001; **357**:617-623.
26 Ambros V. The functions of animal microRNAs. *Nature* 2004; **431**:350-355.
27 Bartel DP. MicroRNAs: genomics, biogenesis, mechanism, and function. *Cell* 2004; **116**:281-297.
28 Jiang L, Mao P, Song L, *et al*. miR-182 as a prognostic marker for glioma progression and patient survival. *Am J Pathol* 2010; **177**:29-38.
29 Verstrepen L, Carpentier I, Verhelst K, Beyaert R. ABINs: A20 binding inhibitors of NF-kappa B and apoptosis signal-

ing. *Biochem Pharmacol* 2009; **78**:105-114.
30 Shembade N, Harhaj NS, Parvatiyar K, *et al.* The E3 ligase ITCH negatively regulates inflammatory signaling pathways by controlling the function of the ubiquitin-editing enzyme A20. *Nat Immunol* 2008; **9**:254-262.
31 Lee J, Kotliarova S, Kotliarov Y, *et al*. Tumor stem cells derived from glioblastomas cultured in bFGF and EGF more closely mirror the phenotype and genotype of primary tumors than do serum-cultured cell lines. *Cancer Cell* 2006; **9**:391-403.
32 Mariani L, Beaudry C, McDonough WS, *et al*. Glioma cell motility is associated with reduced transcription of proapoptotic and proliferation genes: a cDNA microarray analysis. *J Neurooncol* 2001; **53**:161-176.
33 Hoelzinger DB, Mariani L, Weis J, *et al*. Gene expression profile of glioblastoma multiforme invasive phenotype points to new therapeutic targets. *Neoplasia* 2005; **7**:7-16.
34 Guo Q, Dong H, Liu X, *et al*. A20 is overexpressed in glioma cells and may serve as a potential therapeutic target. *Expert Opin Ther Targets* 2009; **13**:733-741.
35 Hjelmeland AB, Wu Q, Wickman S, *et al*. Targeting A20 decreases glioma stem cell survival and tumor growth. *PLoS Biol* 2010; **8**:e1000319.
36 Shembade N, Harhaj NS, Liebl DJ, Harhaj EW. Essential role for TAX1BP1 in the termination of TNF-alpha-, IL-1- and LPS-mediated NF-kappaB and JNK signaling. *EMBO J* 2007; **26**:3910-3922.
37 Shembade N, Parvatiyar K, Harhaj NS, Harhaj EW. The ubiquitin-editing enzyme A20 requires RNF11 to downregulate NF-kappaB signalling. *EMBO J* 2009; **28**:513-522.
38 Karin M. Nuclear factor-kappaB in cancer development and progression. *Nature* 2006; **441**:431-436.
39 Hayden MS, Ghosh S. Shared principles in NF-kappaB signaling. *Cell* 2008; **132**:344-362.
40 Bremm A, Freund SM, Komander D. Lys11-linked ubiquitin chains adopt compact conformations and are preferentially hydrolyzed by the deubiquitinase Cezanne. *Nat Struct Mol Biol* 2010; **17**:939-947.
41 Dynek JN, Goncharov T, Dueber EC, *et al*. c-IAP1 and UbcH5 promote K11-linked polyubiquitination of RIP1 in TNF signaling. *EMBO J* 2010; **29**:4198-4209.
42 Narducci MG, Arcelli D, Picchio MC, *et al*. MicroRNA profiling reveals that miR-21, miR486 and miR-214 are upregulated and involved in cell survival in Sézary syndrome. *Cell Death Dis* 2011; **2**:e151.
43 Mosakhani N, Sarhadi VK, Borze I, *et al*. MicroRNA profiling differentiates colorectal cancer according to KRAS status. *Genes Chromosomes Cancer* 2012; **51**:1-9.
44 Qian S, Ding JY, Xie R, *et al*. MicroRNA expression profile of bronchioalveolar stem cells from mouse lung. *Biochem Biophys Res Commun* 2008; **377**:668-673.
45 Hu Z, Chen X, Zhao Y, *et al*. Serum microRNA signatures identified in a genome-wide serum microRNA expression profiling predict survival of non-small-cell lung cancer. *J Clin Oncol* 2010; **28**:1721-1726.
46 Oh HK, Tan AL, Das K, *et al*. Genomic loss of miR-486 regulates tumor progression and the OLFM4 antiapoptotic factor in gastric cancer. *Clin Cancer Res* 2011; **17**:2657-2667.
47 Betel D, Koppal A, Agius P, Sander C, Leslie C. Comprehensive modeling of microRNA targets predicts functional non-conserved and non-canonical sites. *Genome Biol* 2010; **11**:R90.
48 Hyun S, Lee JH, Jin H, *et al*. Conserved MicroRNA miR-8/miR-200 and its target USH/FOG2 control growth by regulating PI3K. *Cell* 2009; **139**:1096-1108.
49 Small EM, O'Rourke JR, Moresi V, *et al.* Regulation of PI3-kinase/Akt signaling by muscle-enriched microRNA-486. *Proc Natl Acad Sci USA* 2010; **107**:4218-4223.
50 Jiang L, Lin C, Song L, *et al*. MicroRNA-30e* promotes human glioma cell invasiveness in an orthotopic xenotransplantation model by disrupting the NF-κB/IκBα negative feedback loop. *J Clin Invest* 2012; **122**:33-47.
51 Li J, Zhang N, Song LB, *et al*. Astrocyte elevated gene-1 is a novel prognostic marker for breast cancer progression and overall patient survival. *Clin Cancer Res* 2008; **14**:3319-3326.
52 Célérier J, Cruz A, Lamandé N, Gasc JM, Corvol P. Angiotensinogen and its cleaved derivatives inhibit angiogenesis. *Hypertension* 2002; **39**:224-228.

(**Supplementary information** is linked to the online version of the paper on the *Cell Research* website.)